

## Electronic Supporting Information

### Tuning electronic properties of bilayer black phosphorene with twisted angle

Nanshu Liu<sup>1</sup>, Junfeng Zhang<sup>2\*</sup>, Si Zhou<sup>1\*</sup>, Jijun Zhao<sup>1</sup>

*1. Key Laboratory of Materials Modification by Laser, Ion and Electron Beams (Dalian University of Technology), Ministry of Education, Dalian 116024, China*

*2. Research Institute of Materials Science of Shanxi Normal University & Collaborative Innovation Center for Shanxi Advanced Permanent Magnetic Materials and Technology, Linfen 041004, China*

## Contents

<b>Table S1.</b> Interlayer distance ( $d$ ), cohesive energy ( $E_{\text{coh}}$ ) and band gap ( $E_{\text{g}}$ ) calculated by using PBE-D3 and opt88-vdW functionals (in brackets). .....	1
<b>Table S2.</b> Lattice mismatch ( $\delta$ , relative to the bottom BP layer), lattice constants ( $a$ and $b$ ), interlayer distance ( $d$ ), cohesive energy ( $E_{\text{coh}}$ ) and band gap ( $E_{\text{g}}$ ) calculated by using different lattice mismatches for $65.08^\circ$ . .....	2
<b>Scheme S1.</b> Assumption and illustration of the orbital overlap of lone pairs. ....	3
<b>Fig. S1.</b> Computed band structures of the twisted bilayer BP versus twisted angle using opt88-vdW functional. ....	4
<b>Fig. S2</b> Calculated cohesive energy ( $E_{\text{coh}}$ ) using opt88-vdW functional as a function of twisted angle ( $\theta$ ) .....	5
<b>Fig. S3.</b> Forming process of twisted bilayer BP with the angle of $\theta$ . ....	7
<b>Fig. S4.</b> Partial charge density of CBM and VBM for weak coupling systems .....	8
<b>Fig. S5.</b> Partial charge density of CBM and VBM for strong coupling systems .....	9
<b>Fig. S6.</b> Electrostatic potential along $z$ direction for weak coupling systems .....	10
<b>Fig. S7.</b> Electrostatic potential along $z$ direction for strong coupling systems.....	11

---

\*Corresponding authors. Email: [zhangjf@sxnu.edu.cn](mailto:zhangjf@sxnu.edu.cn) (J. Zhang), [sizhou@dlut.edu.cn](mailto:sizhou@dlut.edu.cn) (S. Zhou)

**Table S1.** Interlayer distance ( $d$ ), cohesive energy ( $E_{\text{coh}}$ ) and band gap ( $E_{\text{g}}$ ) calculated by using PBE-D3 and opt88-vdW functionals (in brackets).

	$d$ (Å)	$E_{\text{coh}}$ (eV/atom)	$E_{\text{g}}$ (eV)
AA	3.53 (3.49)	−0.033 (−0.048)	0.38 (0.32)
AB	3.22 (3.14)	−0.042 (−0.061)	0.43 (0.37)
Aδ	3.31 (3.21)	−0.039 (−0.056)	0.65 (0.64)
19.21°	3.35 (3.35)	−0.017 (−0.031)	0.51 (0.48)
24.92°	3.32 (3.31)	0 (−0.017)	0.24 (0.22)
38.42°	3.20 (3.32)	−0.034 (−0.049)	0.58 (0.57)
49.84°	3.19 (3.21)	−0.035 (−0.050)	0.62 (0.60)
54.34°	3.20 (3.19)	−0.003 (−0.026)	0.11 (0.07)
65.08°	3.22 (3.16)	0 (−0.009)	0.58 (0.58)
69.74°	3.24 (3.26)	−0.038 (−0.057)	0.61 (0.60)
85.79°	3.34 (3.27)	−0.023 (−0.049)	0.58 (0.56)
90°	3.40 (3.40)	−0.033 (−0.032)	0.74 (0.73)

**Table S2.** Lattice mismatch ( $\delta$ , relative to the bottom BP layer), lattice constants ( $a$  and  $b$ ), interlayer distance ( $d$ ), cohesive energy ( $E_{\text{coh}}$ ) and band gap ( $E_{\text{g}}$ ) calculated by using different lattice mismatches for 65.08°.

$\delta$ (%)	$a$ (Å)	$b$ (Å)	$d$ (Å)	$E_{\text{coh}}$ (eV/atom)	$E_{\text{g}}$ (eV)
0	9.69	10.45	3.22	0	0.58
0.82	9.70	10.54	3.28	0	0.64
1.64	9.71	10.62	3.28	0.003	0.69
2.46	9.72	10.71	3.29	0.005	0.74
3.27	9.73	10.79	3.31	0.008	0.79
4.09	9.73	10.88	3.29	0.012	0.84
4.91	9.74	10.96	3.29	0.018	0.89

**Scheme S1.** Assumption and illustration of the orbital overlap of lone pairs.

To determine the lone pairs coupling strength ( $\alpha$ ), we briefly assume that:

- The orbitals of lone pairs are sphere-like with a radius ( $R_0$ ) of 3 Å (as shown in **Fig. A1** below);
- $\alpha$  is proportional to the volume overlap of the two spherical orbitals;
- The weak interactions for those with  $r_{ij} > 3.5$  Å can be ignored.

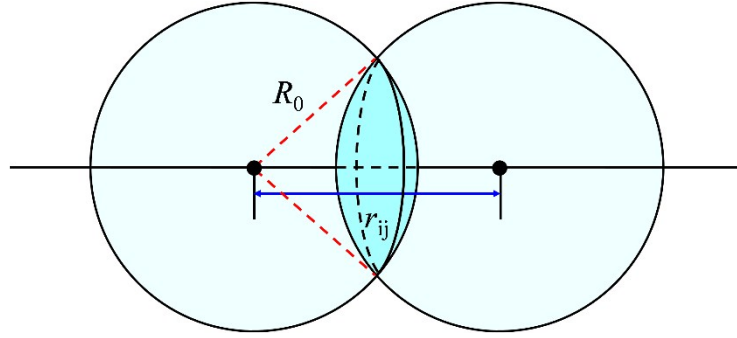


**Fig. A1.** Illustration of the orbital overlap of lone pairs from adjacent P atoms in the upper and lower layers.

The volume overlap of the two spheres with radius of  $R_0$  and distance of  $r_{ij}$  is

$$2\pi(R_0 - r_{ij})^2 \left[ R_0 - \frac{1}{3} \left( R_0 - \frac{r_{ij}}{2} \right) \right], \quad (\text{S1})$$

then  $\alpha$  can be written as:

$$\alpha \sim \begin{cases} \sum_{ij} 2\pi(R_0 - r_{ij})^2 \left[ R_0 - \frac{1}{3} \left( R_0 - \frac{r_{ij}}{2} \right) \right]; r_{ij} \leq 3.5 \text{ \AA} \\ 0; r_{ij} > 3.5 \text{ \AA} \end{cases}, \quad (\text{S2})$$

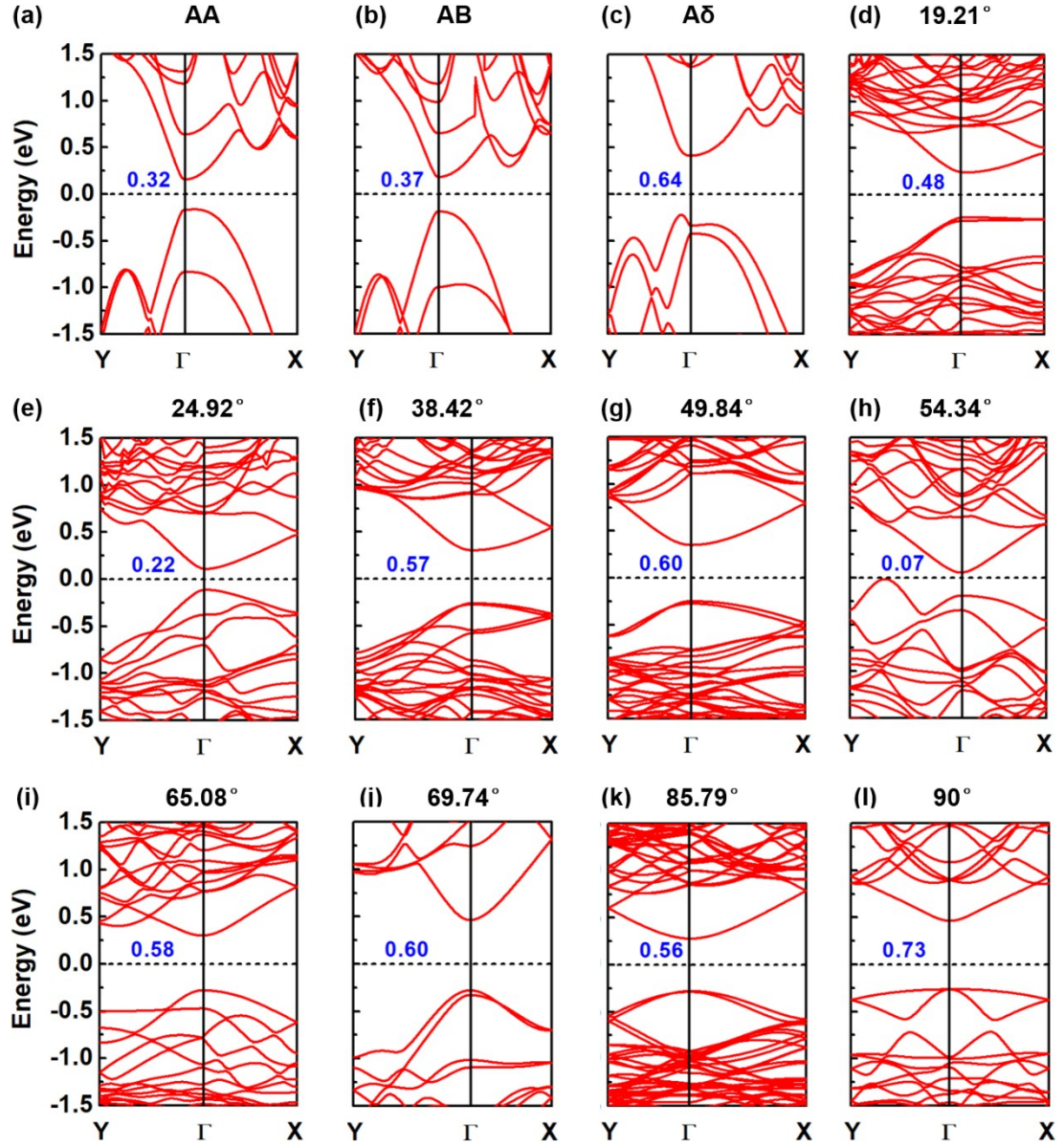


**Fig. S1.** Computed band structures of the twisted bilayer BP versus twisted angle using opt88-vdW functional. The Fermi level is set to zero and the band gap (in eV) is given for each system.

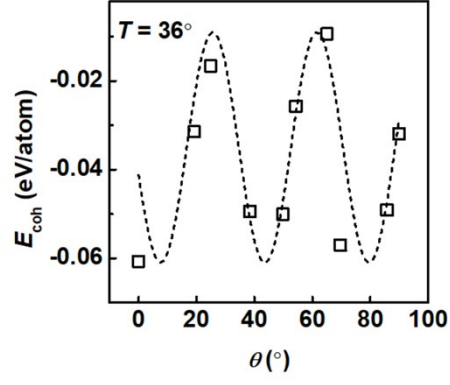


**Fig. S2.** Calculated cohesive energy ( $E_{\text{coh}}$ ) using opt88-vdW functional as a function of twisted angle ( $\theta$ ) with an approximate oscillation period of  $36^{\circ}$ . The dashed lines are visual guide.

The definition and construction of twisted bilayer BP is illustrated by using the  $90^\circ$  system as a representative shown in **Fig. S3**. According to the coincidence-site lattice (CSL) theory,<sup>1</sup> a twisted bilayer BP can be constructed through a relative rotation of the lattice vectors of the two layers, which is consisted by a 2D rotation operator  $R$  and a rigid transition operator  $T$ . We first started from an AA stacking, whose top layer is vertically placed on the bottom BP layer without any displacement. In the case of a twisted bilayer BP, when the top layer of AA stacking is rotated around the original point  $O$  relative to the bottom BP layer under the  $R(\theta)$  operator, coincidence sites will emerge at a specified angle. Then, a rigid transition operator  $T$  was applied to construct the twisted supercell, resulting a Moiré superlattice. In general, the whole operators can be expressed in the following form as:

$$\mathbf{r} = R(\theta)(\mathbf{r}_1 - \mathbf{r}_0) + T(t_1, t_2) \quad (t_1, t_2 \in R^*) \quad (\text{S3})$$

where  $\mathbf{r}_1 - \mathbf{r}_0$  is an in-plane superlattice vector in the bottom BP layer relative to the original point  $O$ , and the rigid translation operator  $T(t_1, t_2)$  is

$$T(t_1, t_2) = t_1 \mathbf{a}_1 + t_2 \mathbf{a}_2 + h \mathbf{a}_3 / |\mathbf{a}_3| \quad (t_1, t_2 \in R^*) \quad (\text{S4})$$

where  $\mathbf{a}_1$  and  $\mathbf{a}_2$  are the two orthorhombic basis vectors along the zigzag and armchair directions, respectively,  $\mathbf{a}_3$  is along the out-of-plane direction,  $h$  denotes the distance between lamellas of a twisted BP layer.

Using the above analyses, twisted bilayer BP with various angles can be constructed by controlling the rotation operator  $R$ . In practice, we started from two pieces of pristine BP domains with sufficiently large size and placed one on the top of another. By gradually rotating the top domain and fixing the bottom one, one can determine the rotation operator  $R$  of the twisted angle (see **Fig. S3** for detail) once the 2D lattices of the two layers roughly overlap with each other.

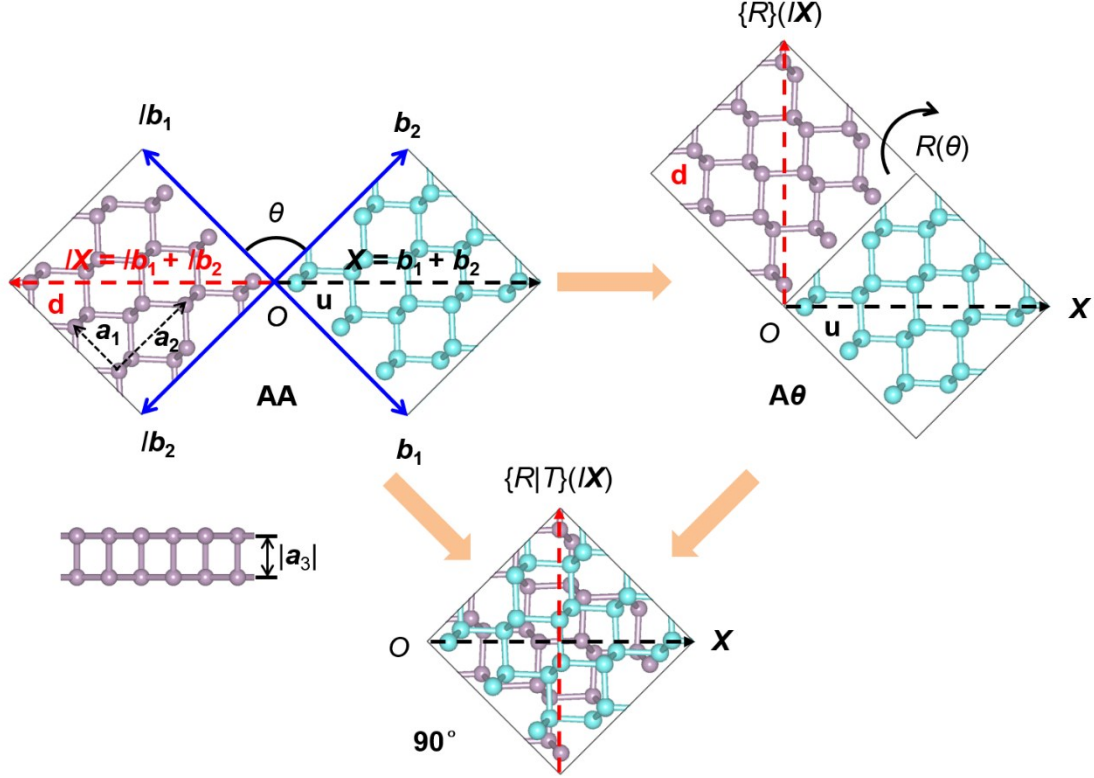


**Fig. S3.** Forming process of twisted bilayer BP with the angle of  $\theta$ .  $R$  indicates a 2D rotation operator,  $T$  is a rigid translation operator, and  $I$  is an inversion operator, respectively.  $\mathbf{a}_1$  and  $\mathbf{a}_2$  are the two orthorhombic basis vectors along the zigzag and armchair directions,  $\mathbf{a}_3$  is along the out-of-plane direction.  $\mathbf{b}_1$  and  $\mathbf{b}_2$  are the two lattice basis vectors of the twisted bilayer BP supercell mapped by  $\mathbf{X} = \mathbf{b}_1 + \mathbf{b}_2$ . For simplicity, we used  $\theta = 90^\circ$  as an example. The P atoms in the upper and lower layers are shown in cyan and purple colors, respectively.



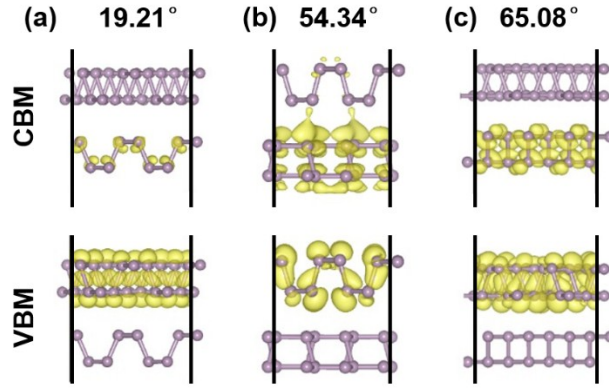


**Fig. S4.** Partial charge density of CBM and VBM for weak coupling systems: (a)  $\theta = 19.21^\circ$ , (b)  $54.34^\circ$ , and (c)  $65.08^\circ$ , respectively. The isosurface value is  $1.2 \times 10^{-3} e\text{\AA}^{-3}$ .

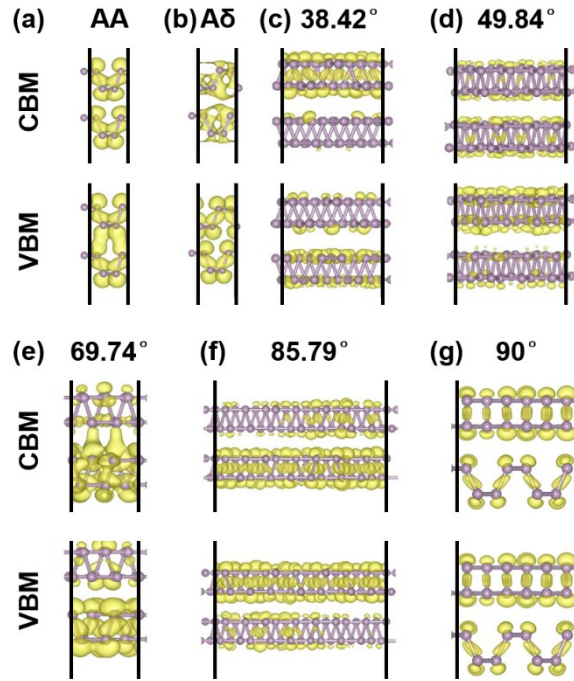


**Fig. S5.** Partial charge density of CBM and VBM for strong coupling systems: (a) AA, (b)  $A\delta$ , and (c)  $\theta = 38.42^\circ$ , (d)  $49.84^\circ$ , (e)  $69.74^\circ$ , (f)  $85.79^\circ$ , and (g)  $90^\circ$ , respectively. The isosurface value is  $1.2 \times 10^{-3} e\text{\AA}^{-3}$ .

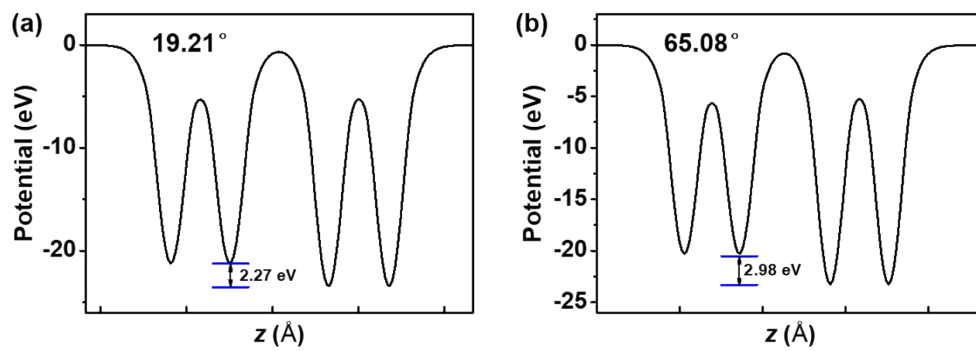


**Fig. S6.** Electrostatic potential along  $z$  direction for weak coupling systems: (a)  $\theta = 24.92^\circ$  and (b)  $65.08^\circ$ , respectively.

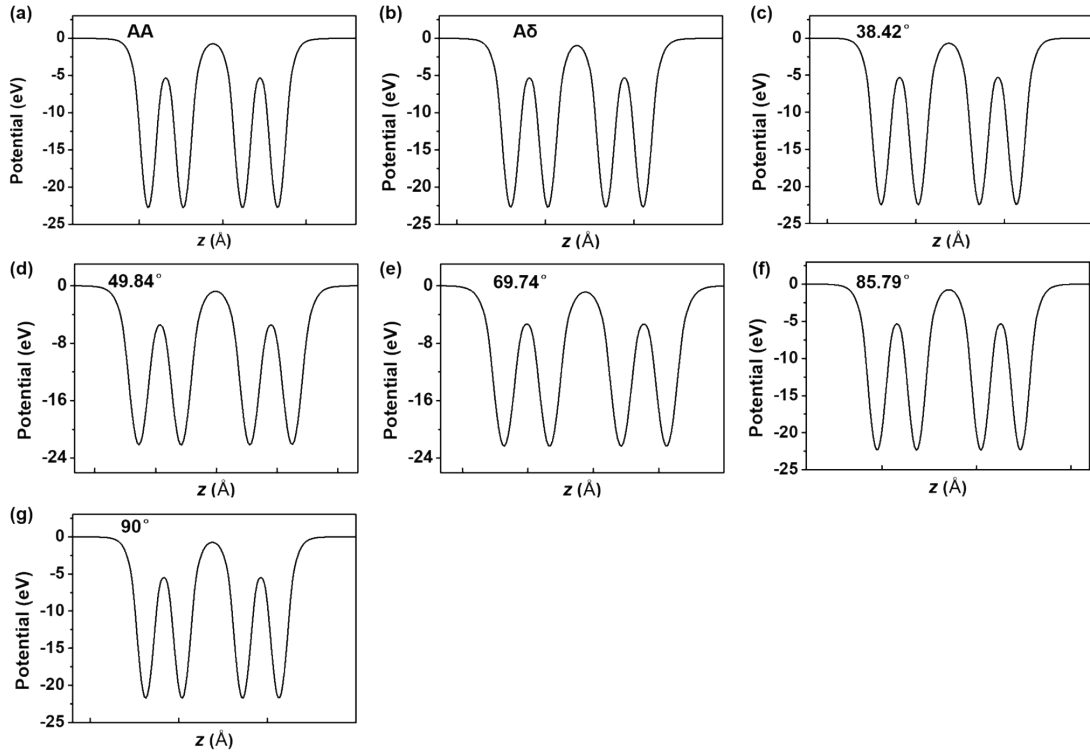


**Fig. S7.** Electrostatic potential along  $z$  direction for strong coupling systems: (a) AA, (b)  $A\delta$ , and (c)  $\theta = 38.42^\circ$ , (d)  $49.84^\circ$ , (e)  $69.74^\circ$ , (f)  $85.79^\circ$ , and (g)  $90^\circ$ , respectively, respectively.

## Reference

1. W. Bollmann, *Crystal defects and crystalline interfaces*, Springer Science & Business Media, 2012.